HOKKAIDO UNIVERSITY

Title	Large thickness dependence of the carrier mobility in a transparent oxide semiconductor, La-doped BaSnO3
Author(s)	Sanchela, Anup V.; Wei, Mian; Zensyo, Haruki; Feng, Bin; Lee, Joonhyuk; Kim, Gowoon; Jeen, Hyoungjeen; Ikuhara, Yuichi; Ohta, Hiromichi
Citation	Applied physics letters, 112(23), 232102 https://doi.org/10.1063/1.5033326
Issue Date	2018-06-04
Doc URL	http://hdl.handle.net/2115/74553
Rights	This article may be downloaded for personal use only. Any other use requires prior permission of the author and AIP Publishing.The following article appeared in Anup V. Sanchela, Mian Wei, Haruki Zensyo, Bin Feng, Joonhyuk Lee, Gowoon Kim, Hyoungjeen Jeen, Yuichi Ikuhara, and Hiromichi Ohta. Large thickness dependence of the carrier mobility in a transparent oxide semiconductor, La-doped BaSnO3. Appl. Phys. Lett. 112, 232102 (2018) and may be found at https://doi.org/10.1063/1.5033326.
Type	article
File Information	1.5033326.pdf

Instructions for use

Large thickness dependence of the carrier mobility in a transparent oxide semiconductor, La-doped BaSnO$_3$

Anup V. Sanchela, Mian Wei, Haruki Zensyo, Bin Feng, Joonhyuk Lee, Gowoon Kim, Hyoungjeen Jeen, Yuichi Ikuhara, and Hiromichi Ohta

Articles you may be interested in

Controlling surface carrier density by illumination in the transparent conductor La-doped BaSnO$_3$
Applied Physics Letters **112**, 181603 (2018); 10.1063/1.5020716

Chemical intermixing at oxide heterointerfaces with polar discontinuity
Applied Physics Letters **112**, 231601 (2018); 10.1063/1.5027796

High-mobility BaSnO$_3$ grown by oxide molecular beam epitaxy
APL Materials **4**, 016106 (2016); 10.1063/1.4939657

Interface energy band alignment at the all-transparent p-n heterojunction based on NiO and BaSnO$_3$
Applied Physics Letters **112**, 171605 (2018); 10.1063/1.5029422

Stability of the oxygen vacancy induced conductivity in BaSnO$_3$ thin films on SrTiO$_3$
Applied Physics Letters **111**, 172102 (2017); 10.1063/1.4996548

High quality gate dielectric/MoS$_2$ interfaces probed by the conductance method
Applied Physics Letters **112**, 232101 (2018); 10.1063/1.5028404

Large thickness dependence of the carrier mobility in a transparent oxide semiconductor, La-doped BaSnO₃

Anup V. Sanchela,[1,a)] Mian Wei,[2] Haruki Zensyo,[3] Bin Feng,[4] Joonhyuk Lee,[5] Gowoon Kim,[5] Hyoungjeen Jeen,[5] Yuichi Ikuhara,[4] and Hiromichi Ohta[1,2,a)]

[1]*Research Institute for Electronic Science, Hokkaido University, N20W10, Kita, Sapporo 001-0020, Japan*
[2]*Graduate School of Information Science and Technology, Hokkaido University, N14W9, Kita, Sapporo 060-0814, Japan*
[3]*School of Engineering, Hokkaido University, N14W9, Kita, Sapporo 060-0814, Japan*
[4]*Institute of Engineering Innovation, The University of Tokyo, 2-11-16 Yayoi, Bunkyo, Tokyo 113-8656, Japan*
[5]*Department of Physics, Pusan National University, Busan 46241, South Korea*

In this study, we report that the carrier mobility of 2%-La-doped BaSnO₃ (LBSO) films on (001) SrTiO₃ and (001) MgO substrates strongly depends on the thickness, whereas it is unrelated to the film/substrate lattice mismatch (+5.4% for SrTiO₃ and −2.3% for MgO). The films exhibited large differences in lattice parameters, lateral grain sizes (∼85 nm for SrTiO₃ and ∼20 nm for MgO), surface morphologies, threading dislocation densities, and misfit dislocation densities. However, the mobility dependences on the film thickness in both cases were almost the same, saturating at ∼100 cm² V⁻¹ s⁻¹, while the charge carrier densities approached the nominal carrier concentration (=[2% La³⁺]). Our study clearly indicates that the carrier mobility of LBSO films strongly depends on the thickness. These results would be beneficial for understanding the carrier transport properties and fruitful to further enhance the mobility of LBSO films. *Published by AIP Publishing.*
https://doi.org/10.1063/1.5033326

Transparent oxide semiconductors (TOSs) showing high optical transparency and high electrical conductivity have been applied as active materials in wide-scale advanced electronic device applications.[1,2] Recently, there has been growing interest on La-doped BaSnO₃ (LBSO; bandgap, E_g ∼ 3.5 eV) with a cubic perovskite structure (a = 4.115 Å) as a novel TOS because flux-grown LBSO single crystals exhibited a very high mobility of 320 cm² V⁻¹ s⁻¹ (carrier concentration, 8×10^{19} cm⁻³) at room temperature (RT).[3,4] Such high mobility is originated from its small carrier effective mass (m^* = 0.40 m_e[5]) and long carrier relaxation time.[6] Therefore, many researchers have tried to prepare high mobility LBSO epitaxial films to date, but the observed mobility has been low compared to that of single crystals.[7–16]

Recently, Paik *et al.* obtained the highest mobility of 183 cm² V⁻¹ s⁻¹ in a LBSO film on DyScO₃ (a = 3.943 Å and Δa = +4.2%).[7] Raghavan *et al.* also achieved high mobilities of 150 cm² V⁻¹ s⁻¹ and 100 cm² V⁻¹ s⁻¹ in LBSO films deposited by the high purity molecular beam epitaxy (MBE) technique on PrScO₃ (a = 4.026 Å and Δa = +2.18%) and SrTiO₃, respectively.[8] Lebens-Higgins *et al.* reported mobility values up to 81 cm² V⁻¹ s⁻¹ in LBSO films grown on TbScO₃ (110) (a = 3.958 Å and Δa = +3.97%) by MBE.[9] A low mobility value of 10 cm² V⁻¹ s⁻¹ was also reported by Wadekar *et al.* in a LBSO film on SmScO₃ (110) (a = 3.991 Å and Δa = +3.1%).[10] These studies attributed the origin of the low mobility to the misfit/threading dislocations, which are generated from a large lattice mismatch (Δa) at the film/substrate interface (i.e., Δa = +5.4% for the LBSO/SrTiO₃ interface).[11–14]

In order to minimize Δa, a buffer layer deposition on a substrate was also investigated.[15–20] Shin *et al.* used an undoped BaSnO₃ film as a buffer layer (150 nm thick) on MgO by the pulsed laser deposition (PLD) technique and obtained a mobility of 97.2 cm² V⁻¹ s⁻¹.[17] Another study by Shiogai *et al.* reported a mobility of 80 cm² V⁻¹ s⁻¹ with (Sr, Ba)SnO₃ buffer (200-nm-thick) deposited by PLD on SrTiO₃.[15] Lee *et al.* have used the flux grown undoped BaSnO₃ (001) single crystal as a substrate, but the resulting mobility was <100 cm² V⁻¹ s⁻¹.[16] These contradict the hypothesis regarding the misfit/threading dislocations since there was almost no lattice mismatch between the substrate and the film.

Several studies suggest that cation off-stoichiometry or cation mixing can introduce charge point defects[21–23] and dislocations, which act as scattering sources and thus suppress the mobility. However, the origin of the limited electron mobility in LBSO thin films has not been clearly explained to date, and a fundamental study on other factors such as the film thickness is required to understand this phenomenon. Therefore, in this study, we analyzed the structural and electrical features of epitaxial LBSO (La₀.₀₂Ba₀.₉₈SnO₃) films with various thicknesses (14–1040 nm), which were grown on (001) perovskite SrTiO₃ (Δa = +5.4%) and non-perovskite (001) MgO (Δa = −2.3%) by PLD.

Here, we report that the carrier mobility of the LBSO films strongly depends on the thickness, whereas it is unrelated to the lattice mismatch. Although we observed large differences in lattice parameters, lateral grain size, the density of threading dislocations, the surface morphology, and the density of misfit dislocations, the mobility increased almost simultaneously with the thickness in both cases and saturated at ∼100 cm² V⁻¹ s⁻¹, together with approaching to

---

a)Authors to whom correspondence should be addressed: anup.sanchela@es.hokudai.ac.jp and hiromichi.ohta@es.hokudai.ac.jp
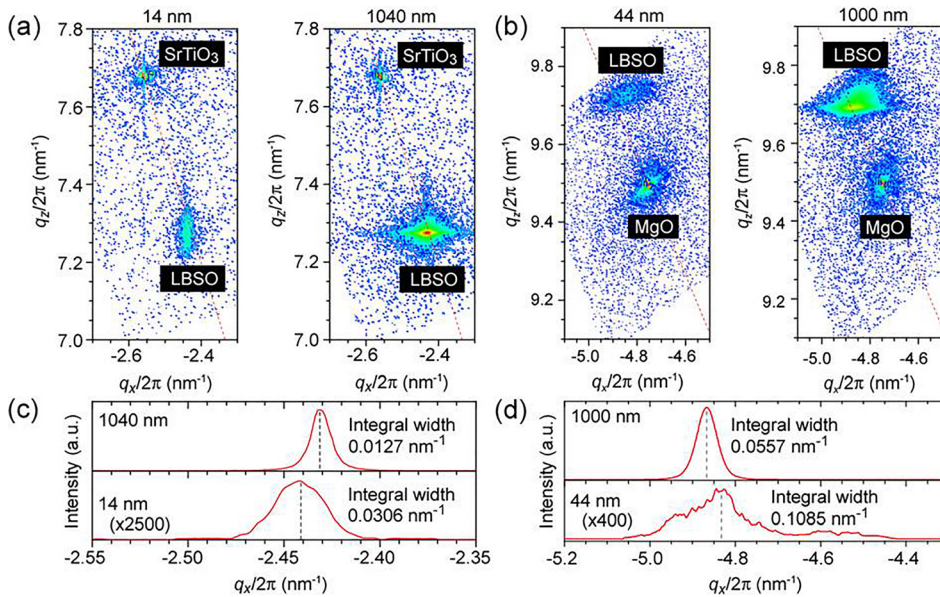
FIG. 1. Crystallographic characterization of the LBSO epitaxial films grown on (001) $SrTiO_3$ and (001) MgO substrates. X-ray reciprocal space mapping around 103 LBSO on (a) (001) $SrTiO_3$ substrates (14-nm-thick and 1040-nm-thick films) and (b) (001) MgO substrates (44-nm-thick and 1000-nm-thick films) is shown. The red dotted lines show cubic symmetry. Cross-sectional intensity profiles of the 103 LBSO peak on (c) (001) $SrTiO_3$ substrates [from (a)] and (d) (001) MgO substrates [from (b)].

the nominal carrier concentration (=[2% La^{3+}]), clearly indicating that the behavior of mobility depends on the film thickness. The present results would be beneficial to understand the behavior of mobility and fruitful to further enhance the mobility of La-doped $BaSnO_3$ thin films.

Epitaxial $La_{0.02}Ba_{0.98}SnO_3$ films with thicknesses varying from 14 nm to 1.04 μm were heteroepitaxially grown on (001) $SrTiO_3$ and (001) MgO single crystal substrates by the PLD technique using a KrF excimer laser ($\lambda = 248$ nm, fluence $\sim$2 J cm^{-2} pulse^{-1}, 10 Hz). The temperatures during the film growth were 700 °C for $SrTiO_3$ substrates and 750 °C for MgO substrates, while the oxygen pressure was kept at 10 Pa. In the case of $SrTiO_3$ substrates, the LBSO films were annealed at 1200 °C in air to obtain atomically smooth surfaces.[5,15]

High-resolution X-ray diffraction (Cu Kα_1, ATX-G, Rigaku Co.) measurements revealed that the LBSO films were heteroepitaxially grown on (001) $SrTiO_3$ substrates and (001) MgO substrates with a cube-on-cube epitaxial relationship. The film thicknesses were determined from the Kiessig fringes or Pendellosung fringes. The surface morphology was investigated using an atomic force microscope (AFM, Nanocute, Hitachi High Tech.). The stepped and terraced surface was observed on the film grown on a (001) $SrTiO_3$ substrate (Fig. S1(a) in the supplementary material), whereas very tiny grains were observed in the film grown on a (001) MgO substrate (Fig. S1(b) in the supplementary material). The AFM images show that the films grown on $SrTiO_3$ and MgO have very different surface morphologies.

In order to elaborate the structural differences in more detail, X-ray reciprocal space mappings (RSMs) were performed around the asymmetric 103 diffraction spots of $BaSnO_3$ with the 103 diffraction spots of $SrTiO_3$ [Fig. 1(a)] and the 204 diffraction spot of MgO [Fig. 1(b)]. While the $q_x/2\pi$ peak position of $BaSnO_3$ and the substrate are different from each other, they both are located nearby the red dotted line (cubic), indicating incoherent epitaxial growth occurred in both cases. In order to determine the lateral grain size (D), we plotted the cross-sectional peak intensity as a function of $q_x/2\pi$. In the case of the $SrTiO_3$ substrate, an integral width

of 0.0306 nm^{-1} was obtained for the 14-nm-thick film, whereas that of 0.0127 nm^{-1} was obtained for the 1040-nm-thick film [Fig. 1(c)]. In the case of the MgO substrate, an integral width of 0.1085 nm^{-1} was obtained for the 44-nm-thick film, whereas that of 0.0557 nm^{-1} was obtained for the 1000-nm-thick film [Fig. 1(d)].

Using the 103 diffraction spots, we calculated the average lattice parameters, $(a^2 \cdot c)^{1/3}$, of the LBSO films grown on $SrTiO_3$ and MgO substrates [Fig. 2(a)], where a and c are the in-plane and the out-of-plane lattice parameters, respectively. The $(a^2 \cdot c)^{1/3}$ values of the films on $SrTiO_3$ and MgO substrates initially showed opposite behaviors; $(a^2 \cdot c)^{1/3}$ of the films on MgO was larger than the bulk, whereas that of the films on $SrTiO_3$ was smaller than the bulk, which are probably attributed to the differences in the lattice mismatch. On both substrates, the $(a^2 \cdot c)^{1/3}$ values were nearly similar when the thickness was greater than 300 nm. We then calculated the lateral grain size [$D =$ (integral width in the $q_x/2\pi$ direction of the RSM)$^{-1}$] of the LBSO films grown on $SrTiO_3$ and MgO substrates as shown in Fig. 2(b). The lateral grain sizes were quite different as the LBSO films on $SrTiO_3$ exhibited a maximum grain size of $\sim$85 nm, whereas the grains in the LBSO films on MgO were 20 nm or less.

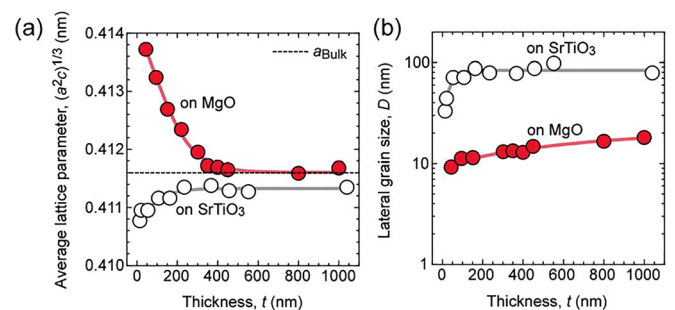The microstructure of the LBSO films was characterized by high-angle annular dark-field scanning transmission

FIG. 2. Thickness dependence of the crystal quality of the LBSO epitaxial films grown on (001) $SrTiO_3$ and (001) MgO substrates. (a) Average lattice parameters $(a^2 c)^{1/3}$ and (b) lateral grain size (D) of the LBSO films grown on $SrTiO_3$ (white) and MgO (red). Large differences in the lattice parameters and the lateral grain sizes were observed.
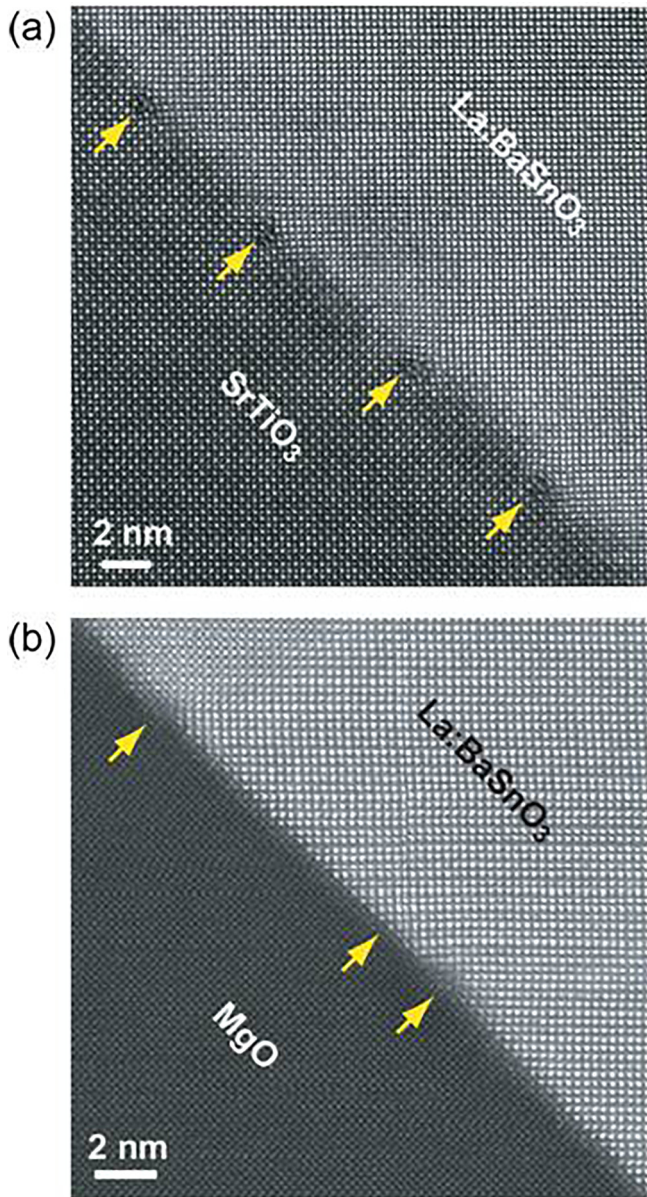
FIG. 3. Cross-sectional HAADF-STEM images for the LBSO epitaxial films. (a) 1040-nm-thick LBSO film grown on a SrTiO$_3$ substrate. (b) 1000-nm-thick LBSO film grown on a MgO substrate. While mismatch dislocations (arrow) are seen periodically ($\sim$7.3 nm) in (a), such periodicity is not clearly seen in (b), indicating the difference of the mismatch dislocation density.

electron microscopy (HAADF-STEM). Figure 3 shows the cross-sectional HAADF-STEM images of (a) the 1.04-μm-thick LBSO/SrTiO$_3$ and (b) the 1-μm-thick LBSO/MgO films. In the case of LBSO/SrTiO$_3$ [Fig. 3(a)], mismatch dislocations (indicated by arrows) are observed periodically at the interface. The spacing of the mismatch dislocation was about 7.3 nm, which is in good agreement with $\Delta a = +5.3\%$. On the other hand, in the case of LBSO/MgO [Fig. 3(b)], mismatch dislocations were not periodic but seemingly occasional. Furthermore, we observed high density threading dislocations in the cross-sectional low-angle annular dark-field (LAADF)-STEM images of the films as shown in Fig. S2 in the supplementary material. The average distance between two threading dislocations is $\sim$100 nm for LBSO/SrTiO$_3$ [Fig. S2(a)] and $\sim$30 nm for LBSO/MgO [Fig. S2(b)], reflecting the lateral grain sizes obtained from the RSMs

($\sim$85 nm for LBSO/SrTiO$_3$ and $\sim$20 nm for LBSO/MgO). Thus, the densities of the threading dislocations are 1.4×10^{10} cm^{-2} for the film on the SrTiO$_3$ substrate and 2.5×10^{11} cm^{-2} for the film on the MgO substrate. These results show that there are several structural differences between the LBSO films on SrTiO$_3$ and MgO substrates, which include the surface morphology, lattice parameter, lateral grain size, density of threading dislocations, and density of misfit dislocations.

The electrical resistivity (ρ), carrier concentration (n), Hall mobility (μ_{Hall}), and thermopower (S) of the LBSO films at room temperature (RT) and low temperatures were measured by the conventional DC four-probe method using an In-Ga alloy electrode with van der Pauw geometry. S-values were measured by creating a temperature difference (ΔT) of $\sim$4 K across the film using two Peltier devices. Two small thermocouples were used to monitor the actual temperatures of each end of the film. The thermo-electromotive force (ΔV) and ΔT were measured simultaneously, and the S-values were obtained from the slope of the ΔV–ΔT plots (correlation coefficient $>$0.9999).

Figure 4 and Tables SI and SII in the supplementary material summarize the electron transport properties of the LBSO films grown on SrTiO$_3$ and MgO substrates at RT. Regarding the overall tendencies, no clear difference was observed from LBSO films deposited on SrTiO$_3$ and MgO substrates. The value of n increased with the increasing thickness and approached the nominal carrier concentration ($=$[2% La^{3+}]). Approximately, 88% La^{3+} dopants were activated and produced conducting electrons for films thicker than 350 nm [Fig. 4(a)]. Similarly, the magnitude of S [Fig. 4(b)], which decreases with increasing n, gradually decreased with the thickness, which is consistent with Fig. 4(a). All values of S were negative, indicating that the LBSO films are n-type semiconductors.[24] In addition, μ_{Hall} increased gradually with the thickness and became constant for films thicker than 350 nm. The highest mobility values were 97.7 cm^2 V^{-1} s^{-1} for 1040 nm thick LBSO/SrTiO$_3$ and 99.2 cm^2 V^{-1} s^{-1} for 450 nm thick LBSO/MgO. The thickness dependence of μ_{Hall} and n in the LBSO films were similar on both SrTiO$_3$ and MgO substrates. In addition, since μ_{Hall} and n of LBSO films thicker than 350 nm do not show a significant dependence on the substrates, the contributions from the structural differences between LBSO/SrTiO$_3$ and LBSO/MgO on the mobility are likely small.

The electron mobility in LBSO films rapidly increased with the thickness. However, the maximum mobility ($\sim$100 cm^2 V^{-1} s^{-1}) was still low compared to the bulk values ($\sim$320 cm^2 V^{-1} s^{-1}). In order to further investigate the suppression of electronic transport properties, we performed x-ray absorption spectroscopy (XAS) around the Sn M$_{4,5}$ edge of a 500-nm-thick LBSO film on the SrTiO$_3$ substrate in the Pohang accelerator laboratory (2A) (Fig. S3 in the supplementary material). Several peaks (A–F) were clearly observed in the XAS spectra. The peaks labeled as B–F are well matched with BaSnO$_3$. However, there is an additional peak from the 2+ valence state of Sn (SnO, peak A). The relative peak intensity A in the surface region was smaller than that of the deep region. Since we did not detect the SnO phase in the film by the XRD measurements and the STEM
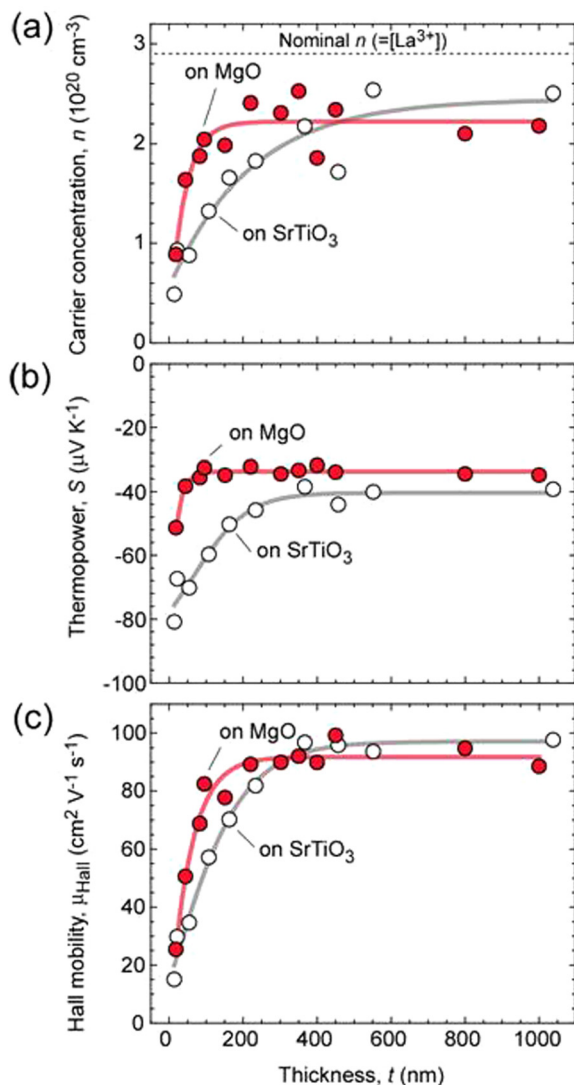
FIG. 4. Thickness dependent electron transport properties of the LBSO epitaxial films at RT. [(a) carrier concentration (n), (b) thermopower (S), and (c) Hall mobility (μ_{Hall})]. No clear differences in the overall tendencies were observed on SrTiO$_3$ and MgO substrates.

observations, the Sn^{2+} ions substitute either the B-site or the A-site of the perovskite BaSnO$_3$. If Sn^{2+} ions substitute the B-site in the LBSO films, the Sn^{2+} should play as electron acceptors and ionized impurities, and they may be related to the suppression of μ_{Hall} and n in the films (compared to bulk values). From these observations, we speculate that the thickness dependence of the electron transport properties originates from the thickness dependence of the Sn^{2+} ion concentration. In order to clarify the formation mechanism of Sn^{2+} ions, a further study is needed.

Finally, we measured the temperature dependence of the electron transport properties of the LBSO films grown on (001) SrTiO$_3$ substrates (Fig. S3 in the supplementary material). Metallic behavior was observed in all the films [Fig. S4(a)], indicating that the Fermi energy is located above the conduction band edge and the films behave as degenerate semiconductors.[14] The values of n for all films were almost temperature independent and similar for films thicker than 350 nm [Fig. S4(b)]. μ_{Hall} increased with decreasing temperature, and the change was more significant for thicker films. The highest μ_{Hall} of 163 cm^2 V^{-1} s^{-1} was observed in the

1040 nm thick LBSO film at 8 K [Fig. S4(c)]. $|S|$ almost linearly decreased with decreasing temperature [Fig. S4(d)], which is typical for degenerate semiconductors.[24]

In summary, we have demonstrated that the electron transport properties of the LBSO films grown on (001) SrTiO$_3$ and (001) MgO substrates show a strong thickness dependence in the range of 14 nm–1040 nm. Although LBSO/SrTiO$_3$ and LBSO/MgO exhibited several structural differences including lattice parameters, lateral grain size, the density of threading dislocations, the surface morphology, and the density of misfit dislocations, these structural discrepancies did not play a major role in the carrier mobility as no clear structure-induced difference was observed in the electron transport properties. μ_{Hall} and n increased with the increasing LBSO film thickness. On both SrTiO$_3$ and MgO substrates, the maximum μ_{Hall} observed was ~100 cm^2 V^{-1} s^{-1}. While the origin of the strong thickness dependence of μ_{Hall} remains unclear, we detected the 2+ valence state of Sn in the XAS spectrum of a 500 nm thick LBSO film. Since Sn^{2+} ions should play not only as electron acceptors but also as ionized impurities, they may increase the scattering cross section of the electrons and contribute to the mobility suppression.[21–23] We hope to clarify the effect of the Sn valence state on the electron mobility of LBSO films in near future.

We believe that our results can provide a guideline for the thickness optimization of high-mobility LBSO films grown on other substrates. This study also provides further insights into the development of LBSO-based electronic devices.

See supplementary material for the topographic AFM, cross-sectional LAADF-STEM, XAS, and temperature dependence of the electron transport properties of the LBSO films.

[1]D. S. Ginley, H. Hosono, and D. C. Paine, *Handbook of Transparent Conductors* (Springer, New York, 2010).
[2]P. Barquinha, R. Martins, L. Pereira, and E. Fortunato, *Transparent Oxide Electronics: From Materials to Devices* (Wiley, West Sussex, 2012).

[3]H. J. Kim, U. Kim, H. M. Kim, T. H. Kim, H. S. Mun, B.-G. Jeon, K. T. Hong, W.-J. Lee, C. Ju, K. H. Kim, and K. Char, "High mobility in a stable transparent perovskite oxide," Appl. Phys. Express **5**, 061102 (2012).

[4]H. J. Kim, U. Kim, T. H. Kim, J. Kim, H. M. Kim, B.-G. Jeon, W.-J. Lee, H. S. Mun, K. T. Hong, J. Yu, K. Char, and K. H. Kim, "Physical properties of transparent perovskite oxides (Ba,La)SnO$_3$ with high electrical mobility at room temperature," Phys. Rev. B **86**, 165205 (2012).

[5]A. V. Sanchela, T. Onozato, B. Feng, Y. Ikuhara, and H. Ohta, "Thermopower modulation clarification of the intrinsic effective mass in transparent oxide semiconductor BaSnO$_3$," Phys. Rev. Mater. **1**, 034603 (2017).

[6]K. Krishnaswamy, B. Himmetoglu, Y. Kang, A. Janotti, and C. G. Van de Walle, "First-principles analysis of electron transport in BaSnO$_3$," Phys. Rev. B **95**, 205202 (2017).

[7]H. Paik, Z. Chen, E. Lochocki, A. Seidner H, A. Verma, N. Tanen, J. Park, M. Uchida, S. Shang, B.-C. Zhou, M. Brützam, R. Uecker, Z.-K. Liu, D. Jena, K. M. Shen, D. A. Muller, and D. G. Schlom, "Adsorption-controlled growth of La-doped BaSnO$_3$ bymolecular-beam epitaxy," APL Mater. **5**, 116107 (2017).

[8]S. Raghavan, T. Schumann, H. Kim, J. Y. Zhang, T. A. Cain, and S. Stemmer, "High-mobility BaSnO$_3$ grown by oxide molecular beam epitaxy," APL Mater. **4**, 016106 (2016).

[9]Z. Lebens-Higgins, D. O. Scanlon, H. Paik, S. Sallis, Y. Nie, M. Uchida, N. F. Quackenbush, M. J. Wahila, G. E. Sterbinsky, D. A. Arena, J. C. Woicik, D. G. Schlom, and L. F. Piper, "Direct observation of electrostatically driven band gap renormalization in a degenerate perovskite transparent conducting oxide," Phys. Rev. Lett. **116**, 027602 (2016).

[10]P. V. Wadekar, J. Alaria, M. O'Sullivan, N. L. O. Flack, T. D. Manning, L. J. Phillips, K. Durose, O. Lozano, S. Lucas, J. B. Claridge, and M. J. Rosseinsky, "Improved electrical mobility in highly epitaxial La:BaSnO$_3$ films on SmScO$_3$ (110) substrates," Appl. Phys. Lett. **105**, 052104 (2014).

[11]C. A. Niedermeier, S. Rhode, S. Fearn, K. Ide, M. A. Moram, H. Hiramatsu, H. Hosono, and T. Kamiya, "Solid phase epitaxial growth of high mobility La:BaSnO$_3$ thin films co-doped with interstitial hydrogen," Appl. Phys. Lett. **108**, 172101 (2016).

[12]K. Ganguly, P. Ambwani, P. Xu, J. S. Jeong, K. A. Mkhoyan, C. Leighton, and B. Jalan, "Structure and transport in high pressure oxygen sputter-deposited BaSnO$_{3-\delta}$," APL Mater. **3**, 062509 (2015).

[13]H. Mun, U. Kim, H. Min Kim, C. Park, T. Hoon Kim, H. Joon Kim, K. Hoon Kim, and K. Char, "Large effects of dislocations on high mobility of epitaxial perovskite Ba$_{0.96}$La$_{0.04}$SnO$_3$ films," Appl. Phys. Lett. **102**, 252105 (2013).

[14]U. Kim, C. Park, T. Ha, R. Kim, H. S. Mun, H. M. Kim, H. J. Kim, T. H. Kim, N. Kim, J. Yu, K. H. Kim, J. H. Kim, and K. Char, "Dopant-site-dependent scattering by dislocations in epitaxial films of perovskite semiconductor BaSnO$_3$," APL Mater. **2**, 056107 (2014).

[15]J. Shiogai, K. Nishihara, K. Sato, and A. Tsukazaki, "Improvement of electron mobilityin La:BaSnO$_3$ thin films by insertion of an atomically flat insulating (Sr,Ba)SnO$_3$ buffer layer," AIP Adv. **6**, 065305 (2016).

[16]W.-J. Lee, H. J. Kim, E. Sohn, T. H. Kim, J.-Y. Park, W. Park, H. Jeong, T. Lee, J. H. Kim, K.-Y. Choi, and K. H. Kim, "Enhanced electron mobility in epitaxial (Ba, La)SnO$_3$films on BaSnO$_3$ (001) substrates," Appl. Phys. Lett. **108**, 082105 (2016).

[17]J. Shin, Y. M. Kim, Y. Kim, C. Park, and K. Char, "High mobility BaSnO$_3$ films and field effect transistors on non-perovskite MgO substrate," Appl. Phys. Lett. **109**, 262102 (2016).

[18]C. Park, U. Kim, C. J. Ju, J. S. Park, Y. M. Kim, and K. Char, "High mobility field effect transistor based on BaSnO$_3$ with Al$_2$O$_3$ gate oxide," Appl. Phys. Lett. **105**, 203503 (2014).

[19]W. Y. Wang, Y. L. Tang, Y. L. Zhu, J. Suriya prakash, Y. B. Xu, Y. Liu, B. Gao, S. W. Cheong, and X. L. Ma, "Atomic mapping of Ruddlesden-Popper faults in transparent conducting BaSnO$_3$-based thin films," Sci. Rep. **5**, 16097 (2015).

[20]A. Prakash, P. Xu, A. Faghaninia, S. Shukla, J. W. Ager, C. S. Lo, and B. Jalan, "Wide band gap BaSnO$_3$ films with room temperature conductivity exceeding 10^4 S cm^{-1}," Nat. Commun. **8**, 15167 (2017).

[21]A. Prakash, P. Xu, X. Wu, G. Haugstad, X. Wang, and B. Jalan, "Adsorption-controlled growth and the influence of stoichiometry on electronic transport in hybrid molecular beam epitaxy-grown BaSnO$_3$ films," J. Mater. Chem. C **5**, 5730 (2017).

[22]Y. Ozaki, D. Kan, and Y. Shimakawa, "Influence of cation off-stoichiometry on structural and transport properties of (Ba, La)SnO$_3$ epitaxial thin films grown by pulsed laser deposition," J. Appl. Phys. **121**, 215304 (2017).

[23]W.-J. Lee, H. J. Kim, J. Kang, D. H. Jang, T. H. Kim, J. H. Lee, and K. H. Kim, "Transparent perovskite barium stannate with high electron mobility and thermal stability," Annu. Rev. Mater. Res. **47**, 391 (2017).

[24]*Materials Aspect of Thermoelectricity*, edited by C. Uher (CRC press, Florida, 2017).